



Nitrogen-Doped CoP Electrocatalysts for Coupled Hydrogen Evolution and Sulfur Generation with Low Energy Consumption

Qingwen Zhou, Zihan Shen, Chao Zhu, Jiachen Li, Zhiyuan Ding, Peng Wang, Feng Pan, Zhiyong Zhang, Haixia Ma, Shuangyin Wang, and Huigang Zhang*

Hydrogen production is the key step for the future hydrogen economy. As a promising H₂ production route, electrolysis of water suffers from high overpotentials and high energy consumption. This study proposes an N-doped CoP as the novel and effective electrocatalyst for hydrogen evolution reaction (HER) and constructs a coupled system for simultaneous hydrogen and sulfur production. Nitrogen doping lowers the d-band of CoP and weakens the H adsorption on the surface of CoP because of the strong electronegativity of nitrogen as compared to phosphorus. The H adsorption that is close to thermos-neutral states enables the effective electrolysis of the HER. Only -42 mV is required to drive a current density of -10 mA cm⁻² for the HER. The oxygen evolution reaction in the anode is replaced by the oxidation reaction of Fe²⁺, which is regenerated by a coupled H₂S absorption reaction. The coupled system can significantly reduce the energy consumption of the HER and recover useful sulfur sources.

Hydrogen production is a large and growing industry. The current use of hydrogen is mainly to produce ammonia and crack heavy oil.^[1] Hydrogen also holds great promise for the energy carrier in future because it is clean and renewable.^[2] Most technologies for H₂ production use fossil fuels, which generate CO₂ eventually and increase the greenhouse gas emission.^[3,4] Electrochemical water splitting is a promising technology for clean H₂ production. However, electrolysis of water is an energy-intensive process. Its energy consumption is not competitive against conventional thermal reforming routes.^[5] To reduce the total energy consumption, the overpotentials of the electrolysis reactions must be reduced and the efficiencies must be increased.^[2,4,6,7]


Q. Zhou, Z. Shen, C. Zhu, Z. Ding, Prof. P. Wang, Prof. H. Zhang
National Laboratory of Solid State Microstructures
College of Engineering and Applied Sciences
Institute of Materials Engineering, and Collaborative Innovation
Center of Advanced Microstructures
Nanjing University
Jiangsu 210093, China
E-mail: hgzhang@nju.edu.cn

J. Li, Prof. H. Ma
Department of Chemical Engineering
Northwest University
Shaanxi 710069, China

Prof. F. Pan
School of Advanced Materials
Peking University
Shenzhen Graduate School
Shenzhen, Guangdong 518055, China

Prof. Z. Zhang
School of Information Science and Technology
Northwest University
Shaanxi 710127, China

Prof. S. Wang
College of Chemistry and Chemical Engineering
Hunan University
Changsha, Hunan 410012, China

 The ORCID identification number(s) for the author(s) of this article can be found under <https://doi.org/10.1002/adma.201800140>.

DOI: 10.1002/adma.201800140

In the cathode of a water electrolyzer, the hydrogen evolution reaction (HER) occurs via $2\text{H}^+ + 2\text{e} = \text{H}_2$.^[8] Currently, noble metal materials (like Pt) have been regarded as the most effective and benchmarking electrocatalysts. However, the cost and scarcity of noble metals hinder the large-scale applications. Cost-effective HER catalysts using earth-abundant elements are highly desirable in order to develop competitive technologies for water splitting. Recent studies revealed that transition-metal phosphides (TMPs, for examples, MoP,^[9] CoP,^[10,11] Ni₂P,^[12] and FeP^[13]) demonstrated promising catalytic properties for the HER.^[14] Among these reported electrocatalysts, cobalt phosphides and their alloy with other TMPs show relatively high HER catalytic activity.^[11,15–17] Jaramillo and co-workers showed that Fe_{0.5}Co_{0.5}P have the high HER activity because of the near-optimal Gibbs free energy of H adsorption.^[17] Chen and co-workers reported that Zn doping could make the Co–Co bridge sites favorable for thermo-neutral H adsorption and significantly reduce the overpotentials of the HER.^[18] These progresses demonstrated an effective approach to design and optimize the HER activity by tuning the electronic structure of catalysts.^[18–22] Furthermore, whether or not an anion doping is able to enhance the electrocatalytic properties of CoP deserves theoretical and experimental studies in order to advance the development of high-performance nonprecious catalysts.

In the anode of a water electrolyzer, oxygen gas evolves. O₂ is not economically as valuable as H₂ in terms of practical

demands.^[23–25] Because the oxygen evolution reaction (OER) exhibits a high electrode potential (1.23 V vs H₂/H⁺) and sluggish kinetics,^[6,23,26] considerable overpotentials have to be applied on the anode, leading to the high energy consumption. If the OER is replaced by a reaction of low electrode potentials (<1.23 V vs H₂/H⁺), the energy consumption decreases. Hydrazine and urea had been studied as the anode sacrificial additive to reduce cell voltages.^[25,27] The oxidation of 5-hydroxymethylfurfural was reported to reduce the anode potentials and at the same time produce value-added chemicals.^[23,24] These strategies push the electrochemical H₂ production toward practical applications. However, the industrial implementation of these technologies requires that the sacrificial additives could be supplied in a large quantity or the anodized products are in high demand and of high value.^[9,23] Hydrogen disulfide widely occurs in natural gas resources, refinery byproducts, and some high concentration H₂S gas fields.^[28] Especially, oil refinery and coal chemicals industries produce a large amount of H₂S, which is detrimental to environments because H₂S is poisonous, flammable, and corrosive.^[29] If the H₂S absorption and conversion are able to be coupled into a high effective electrochemical H₂ production, the HER process will become even more economically viable.

In this study, we first proposed an N-doped CoP electrocatalyst for the HER. Nitrogen doping could modulate the electronic structure of orthorhombic CoP and tune the H adsorption on the CoP surface. Because N has a stronger electronegativity than P, the substitution of N for P leads to the charge transfer of Co to N and lowers the d-band center of Co. The interaction of H atoms on the Co–Co bridge sites is weakened in N-doped CoP as compared to the pristine CoP. The adsorption energy is tuned close to be thermo-neutral. When used as the HER electrocatalyst, the N-CoP could reduce the HER overpotential to –42 mV at a current density of –10 mA cm^{–2}, which is only 10 mV more negative than that of Pt. At last, we demonstrated an electrolyzer using N-CoP as the HER catalyst in the cathode and Fe³⁺/Fe²⁺ as the redox mediator in the anode. Instead of evolving O₂ in the electrolyzer, Fe²⁺ is oxidized to Fe³⁺, which is then reduced to Fe²⁺ by H₂S within an absorption reactor. Hydrogen and sulfur are produced in the electrolyzer and absorption reactor, respectively. The coupled system

significantly lowers the energy consumption of hydrogen production and concurrently recovers the useful sulfur resources.

Figure 1a shows the fabrication procedure of N-CoP on carbon cloth (CC). A hydrothermal route is first employed to coat the Co(OH)F precursor onto CC in autoclaves. The resultant CC@Co(OH)F is then phosphorized with NaH₂PO₂ as the phosphorus source in two gases of pure Ar or Ar/NH₃, yielding CC@CoP or CC@N-CoP, respectively. The experiment details are presented in the Supporting Information. The obtained composites are evaluated as the HER electrocatalysts in a coupled system of electrolytic hydrogen evolution and sulfur production. Figure 1b shows the concept of how electrolysis and absorption reactions are coupled. When hydrogen evolves on the cathode (CC@N-CoP), Fe²⁺ is oxidized to Fe³⁺ on the anode. A Nafion membrane separates the two compartments of the electrolyzer and only allows protons transport between the anode and cathode. The redox couple of Fe³⁺/Fe²⁺ and protons could be regenerated by bubbling H₂S in the absorption reactor via the reaction: Fe³⁺ + H₂S = Fe²⁺ + S↓ + 2H⁺.^[30] After the sulfur precipitates are centrifuged, the separated liquid is recycled to the anode compartment of the electrolyzer.

Figure 2a shows the optical images of CC, CC@Co(OH)F, CC@CoP, and CC@N-CoP. The scanning electron microscopy (SEM) images of CC@Co(OH)F in Figure 2b–d demonstrated that Co(OH)F has the nanowire morphology with the diameter of 100–200 nm. Each nanowire roots on the CC surface and grows along the radial direction of carbon fibers. The X-ray diffraction (XRD) pattern of the CC@Co(OH)F sample in Figure 2i indicates the combination of carbon and crystallized Co(OH)F. After phosphorization, the nanowire morphology (Figure 2e,f) is well retained. Although the crystallinity decreases as shown in Figure 2i, the weak XRD peaks of the phosphorized sample agree with orthorhombic CoP (JCPDS Card No. 29-0497). Figure 3a presents a transmission electron microscopy (TEM) image of a single CoP nanowire. It has a diameter of about 110 nm and straight needle-like shape. The high-resolution TEM (HRTEM) image in Figure 3b indicates that the phosphorized nanowire is polycrystal instead of single crystal. The lattice fringes of 0.247 and 0.284 nm in Figure 3b are indexed to the (111) and (011) planes of CoP. It indicates that Co(OH)F is converted to CoP during the heat treatment.

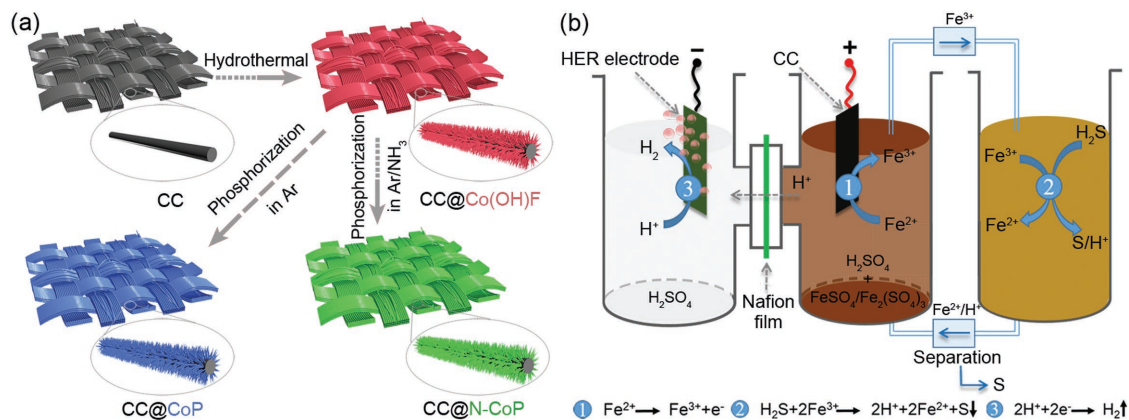


Figure 1. Fabrication of HER catalysts and concept diagram of H₂ and S productions: a) schematic illustration of the fabrication procedure of N-CoP electrocatalyst on CC and (b) concept of the coupled systems of electrolytic hydrogen evolution and sulfur production.

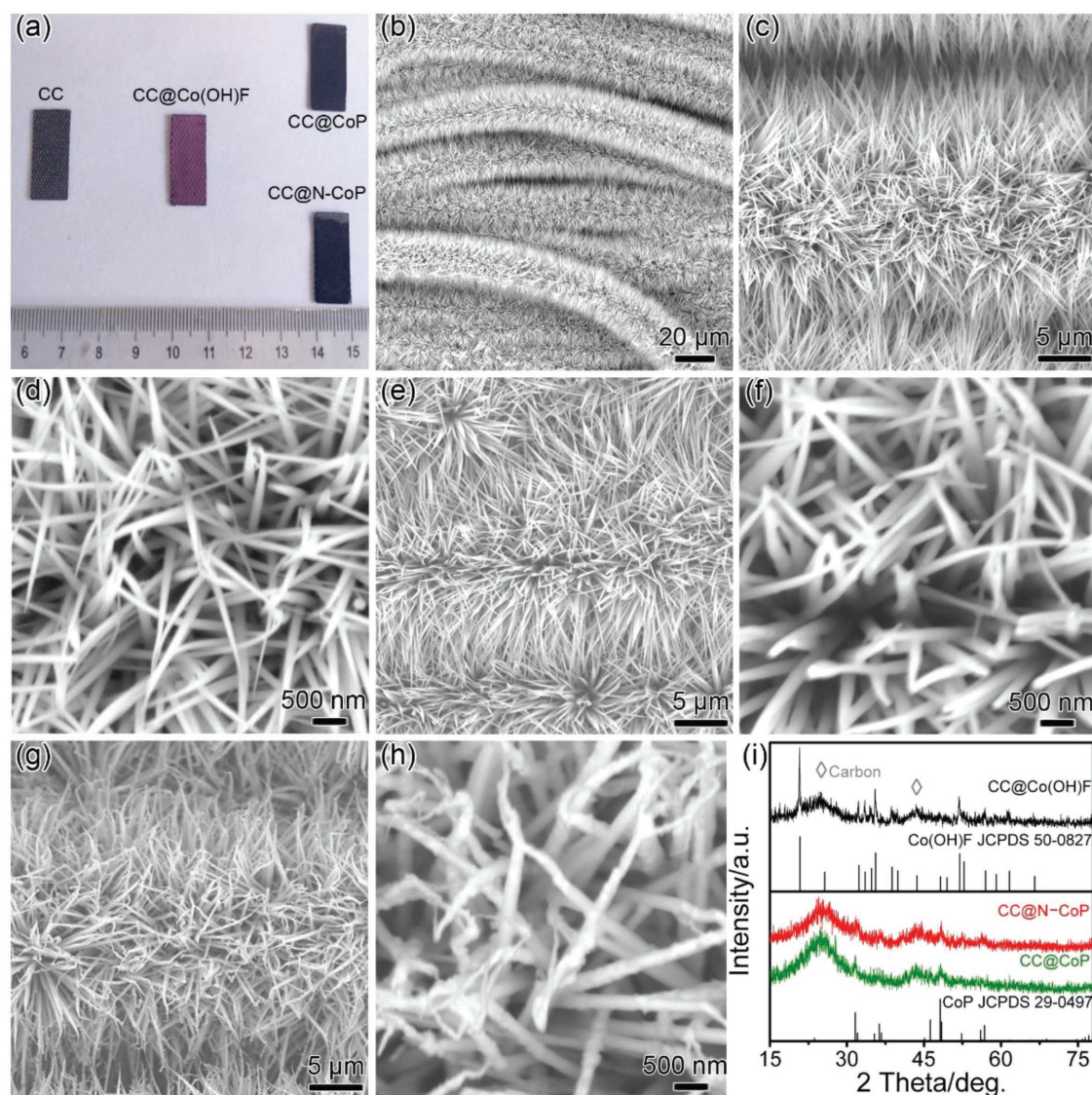


Figure 2. Materials characterizations: a) Optical images of CC, CC@Co(OH)F, CC@CoP, and CC@N-CoP. SEM images of (b–d) CC@Co(OH)F, (e,f) CC@CoP, and (g,h) CC@N-CoP at varied magnifications. i) XRD patterns of CC@Co(OH)F, CC@CoP, and CC@N-CoP.

When NH_3 is introduced into the flowing gas, the resulting nanowires are twisted and some of them folded as shown in Figure 2g,h. These nanowires consist of coarse grains as compared to the smooth shapes of Co(OH)F (Figure 2d) and CoP (Figure 2f). The TEM image in Figure 3d further confirms the coarsen surface of nanowires. The XRD pattern in Figure 2i and lattice fringes in Figure 3e show that the nanowires remain the orthorhombic CoP phase. Energy dispersive X-ray (EDX) spectroscopy is employed to map the elemental distribution along the diameter direction. By comparing the EDX plots in Figure 3c,f, it could be found that nitrogen is doped into the CoP nanowire.

Figure 3g shows the survey scan of the X-ray photoelectron spectroscopy (XPS) of CC@CoP and CC@N-CoP. The distinct N 1s peak at 398.9 eV is attributed to the Co–N bond, which indicates the doping of nitrogen.^[31] In the XPS spectrum of CoP of Figure 3g, the peaks around 778.4 and 793.5 eV are attributed

to the Co $2p_{3/2}$ and $2p_{1/2}$ levels due to spin–orbit splitting, respectively.^[17,32] The Co $2p_{3/2}$ peak of CoP is shifted to higher energy than that of metallic Co (778.2 eV for Co $2p_{3/2}$).^[33] It implies that the oxidation state of Co increases slightly in CoP. It agrees with previous studies.^[32] Figure 3h shows that N doping shifts the binding energy of Co $2p_{3/2}$ from 778.4 to 778.9 eV. It suggests the further increased oxidation state of Co atoms due to nitrogen doping. The P 2p signals in Figure 3i show two wide peaks, which are attributed to phosphide and phosphate, respectively. Previous reports explained that the signals of phosphate result from the superficial oxidation of metal phosphide after exposure to air.^[16,17] The peak at ≈ 130 eV could be fitted into the P $2p_{3/2}$ and P $2p_{1/2}$ signals of phosphides. The increased binding energy of P 2p indicates that after N doping, P atoms partially lose charges as compared to pristine CoP. It is understandable that N has a stronger electronegativity than Co and P. The dopant N attracts electrons from Co and P and

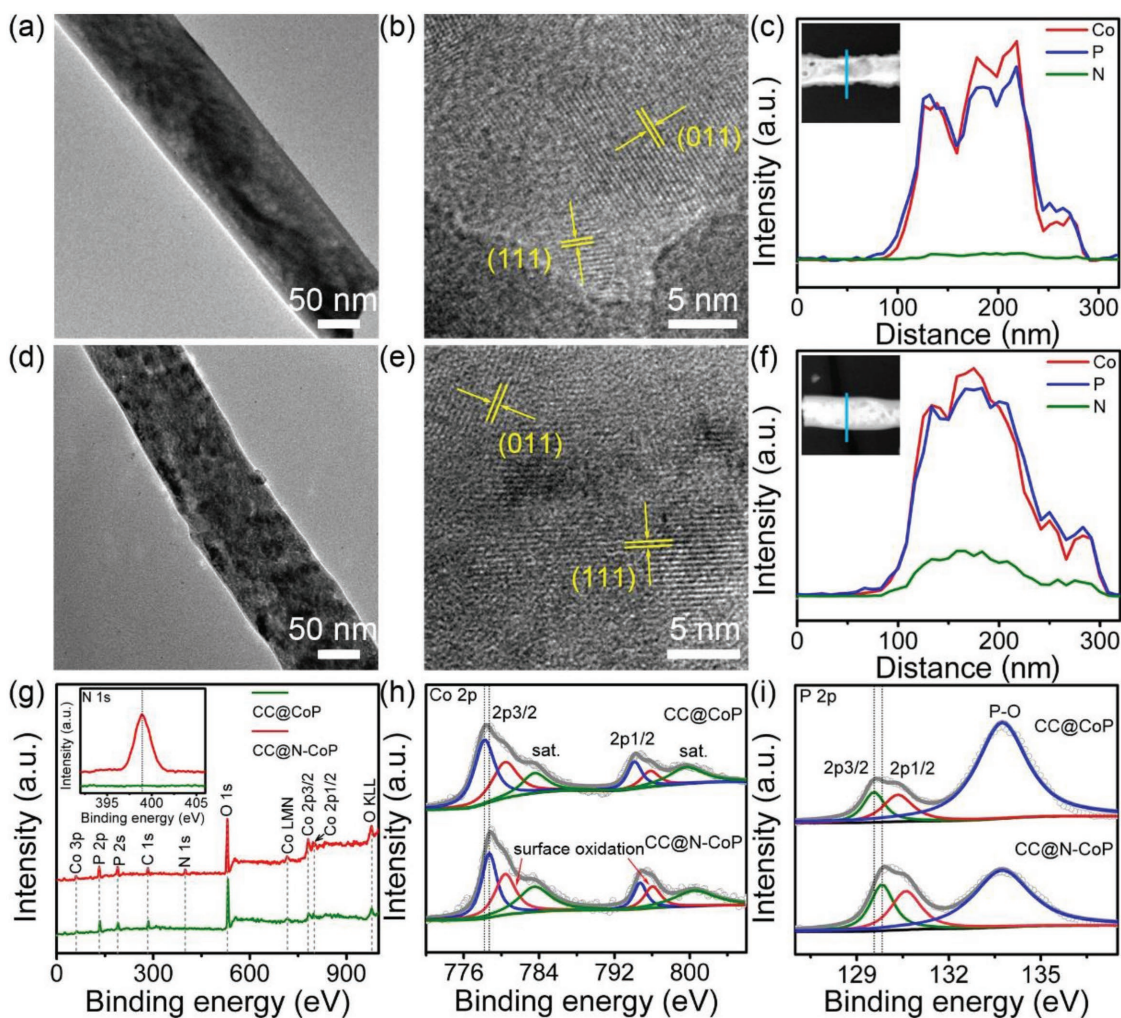


Figure 3. Structural and compositional characterizations: a) TEM image, (b) HRTEM image, and (c) EDX mapping of a CoP nanowire. d) TEM image, (e) HRTEM image, and (f) EDX mapping of N doped CoP nanowire. XPS analysis of (g) survey scan and N 1s, (h) Co 2p, and (i) P 2p spectra in CoP nanowire and N doped CoP nanowire on CC.

modulates the electronic structure of CoP. This modulation may provide an approach to tune the electrocatalytic properties of HER.

The electrocatalytic HER properties of the CoP samples were investigated in 0.5 M H_2SO_4 solution (see Note S1, Supporting Information, for the experimental details). The linear sweep voltammetric (LSV) curves in Figure 4a show that Pt has the best HER electrocatalytic activity. Pt could deliver a current density of -10 mA cm^{-2} at an overpotential of -33 mV . CC without CoP coating barely delivers -0.16 mA cm^{-2} even at an overpotential of -300 mV . For simplicity, the applied overpotential at -10 mA cm^{-2} is denoted as η_{10} . CoP could reduce the η_{10} to -85 mV . CC@N-CoP demonstrates a much lower η_{10} of -42 mV . The inset of Figure 4a and Table S1 in the Supporting Information shows the overpotentials of four samples at varied current densities. CC@N-CoP demonstrates significantly decreased overpotentials at all three current densities as compared to CC@CoP. It indicates that N doping could improve the HER catalytic properties of CoP. The overpotentials required for CC@N-CoP are almost close to those of Pt at

the same current density. We summarized the recent reports about cobalt phosphide electrocatalysts in Table S2 in the Supporting Information. CC@N-CoP is among the most active HER catalysts as compared to recently reported cobalt phosphides (Table S2, Supporting Information) and other transition metal based HER catalysts (Table S3, Supporting Information).

The Tafel plots in Figure 4b shows that the slope of CC@N-CoP is 41.2 mV dec^{-1} , which is lower than that of CC@CoP (50.5 mV dec^{-1}) and near to that of Pt (30.1 mV dec^{-1}). It suggests the enhanced HER activity because of N doping. A low Tafel slope of 41.2 mV dec^{-1} is close to the theoretical value of 39 mV dec^{-1} , implying that the HER on CC@N-CoP may proceed via a Volmer–Heyrovsky mechanism.^[34] The HER rate may be determined by the electrochemical desorption of discharged proton via a Heyrovsky step.^[8,34,35] The Tafel slope of CC@N-CoP is lower than those of most nonprecious catalysts in Tables S2 and S3 in the Supporting Information. The exchange current density (j_0) in Table S1 in the Supporting Information was calculated by extrapolating the intercept of the linear region in the Tafel plots. The j_0 of CC@N-CoP is

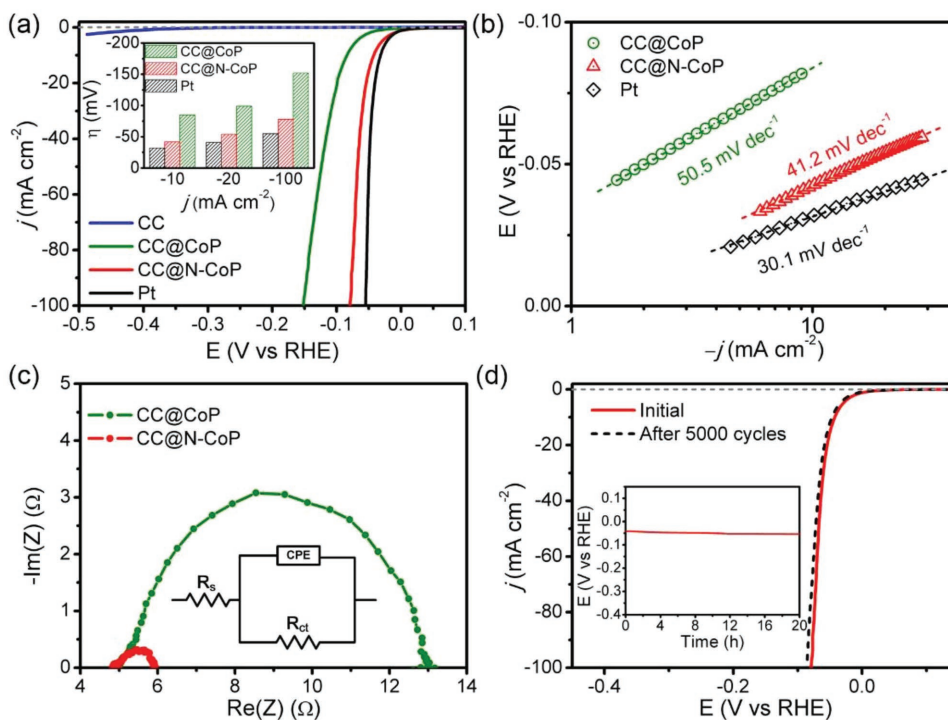


Figure 4. Electrochemical characterizations: HER performances of several electrocatalysts: a) LSV curves of CC, CC@CoP, CC@N-CoP, and Pt (the inset compares overpotentials at varied current densities). b) Tafel plots of CC@CoP, CC@N-CoP, and Pt. c) Nyquist plots of CC@CoP and CC@N-CoP. d) LSV curves of CC@N-CoP prior to and after 5000 cycles (the inset shows the cycling stability of CC@N-CoP at -10 mA cm^{-2} for 20 h).

1.18 mA cm^{-2} , which is over ten times higher than that of CC@CoP (0.11 mA cm^{-2}). It is superior to other nonprecious HER electrocatalysts in Table S3 in the Supporting Information. Figure 4c shows the electrochemical impedance spectroscopy of CC@CoP and CC@N-CoP. The Nyquist plots were fitted with an equivalent circuit in the inset of Figure 4c. CC@N-CoP has the charge transfer resistance (R_{ct}) of $\approx 0.25 \Omega$, which is far lower than that of CC@CoP ($\approx 23.77 \Omega$). It indicates that the N doping enhances the charge transport kinetics of the catalytic HER.^[20,36]

To evaluate the intrinsic catalytic activity, the electrochemically active surface area is estimated by measuring the double-layer capacitance (C_{dl})^[37] and the turnover frequency (TOF) can be calculated according to the previous reports^[38] (see Notes S2 and S3, Supporting Information, for details). Figure S2 in the Supporting Information shows the cyclic voltammograms (CV) curves of CC@N-CoP and CC@CoP at varied scan rates. By fitting the capacitive currents with the scan rates, the C_{dl} values for CC@N-CoP and CC@CoP are estimated to be 49.8 and 45.2 mF cm^{-2} , respectively. At an overpotential of -50 mV , the TOF of N-CoP is calculated to be 0.0199 s^{-1} , which is 6.5 times higher than that of CoP (0.0031 s^{-1}). The stability of electrocatalytic performance is evaluated by repeated CV sweeps and galvanostatic electrolysis. Figure 4d shows that the overpotentials for CC@N-CoP could be well maintained with only a negligible loss of $\approx 5 \text{ mV}$ at -10 mA cm^{-2} after 5000 CV sweeps. During the galvanostatic electrolysis, the overpotentials only increase less than 10 mV after 20 h at -10 mA cm^{-2} . The post-HER analyses show that the chemical and morphological structures of cycled N-CoP are similar to those of as-synthesized N-CoP

before cycling (see Note S4 and Figures S3–S6, Supporting Information). It indicates that CC@N-CoP exhibits good stability in acid solutions. Given the small overpotentials, low Tafel slope, large exchange current density, and high TOF, the N doping significantly improves the catalytic activity of CoP.

To further understand the mechanism of enhanced HER performance, we employ density functional theory (DFT) to calculate the free energy (ΔG_{H^*}) of H adsorption on various catalysts surfaces according to previous reports (see Note S5, Supporting Information).^[1,22,39,40] The ΔG_{H^*} value of Pt (111) is -0.09 eV , which is almost thermo-neutral.^[39,41] Figure 5a presents that the CoP (101) surface has a ΔG_{H^*} value of -0.52 eV on the Co–Co bridge site. The adsorption is relatively strong. After N doping, the ΔG_{H^*} increases to -0.14 eV , which is more thermo-neutral than that of undoped CoP. The thermo-neutral adsorption of H atoms implies the high catalytic activity,^[1,6,42] which is in agreement with the experimental results. Figure 5b presents the atom configuration of H adsorption on the Co–Co bridge site of CoP (101) surface. As shown in Figure 5c, the Bader charge analysis is used to determine the charge transfer quantitatively. In undoped CoP, Co loses about 0.34 electrons to P. The substitution of N for P attracts extra electrons (0.5 e) from the neighboring Co atoms (as shown in the table of Figure 5c) because N has the stronger electronegativity than P. The calculated density of states (DOS) in Figure 5d shows the downshift of d-band due to the N doping. The orbital analysis (Note S6 and Figures S7 and S8, Supporting Information) indicates the strong Co–Co interaction and lowered d-band because of the reduced Co–Co separation caused by stronger N electronegativity. The lowered d-band center predicts the

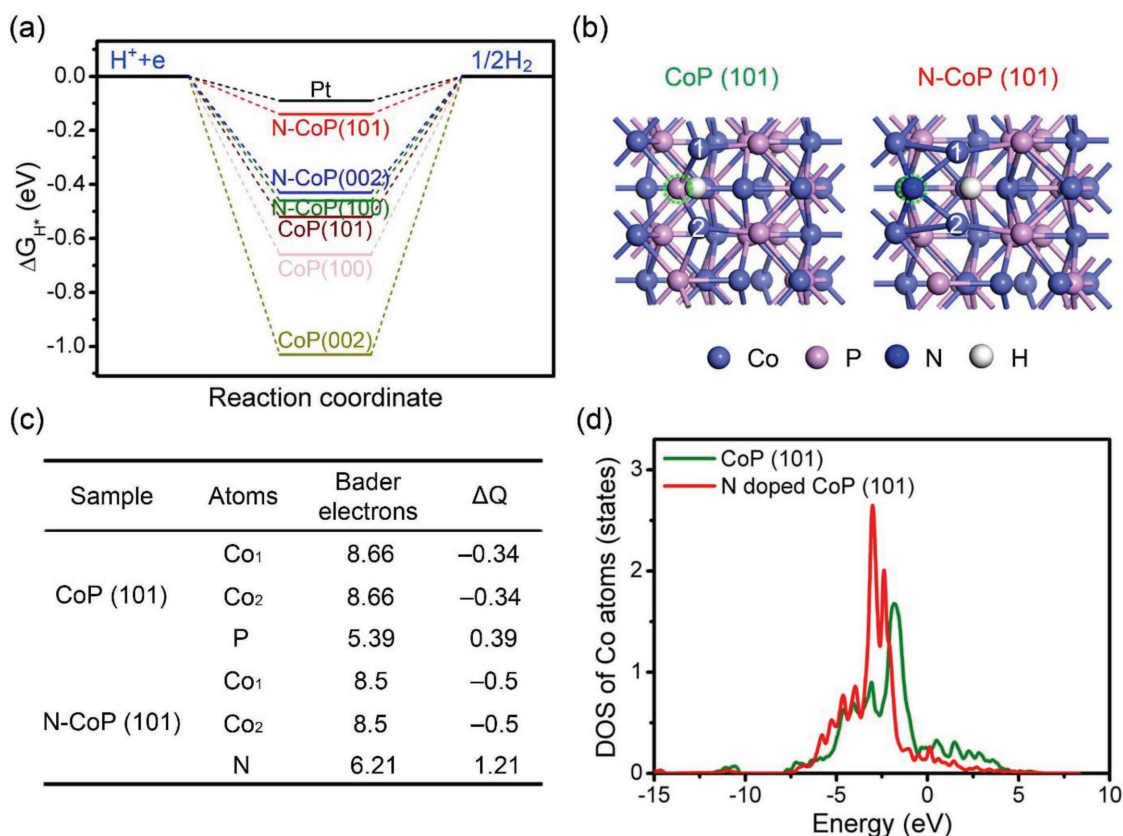


Figure 5. Mechanism investigation: a) Free energy diagram for hydrogen (H^*) adsorption at the Co–Co bridge site on several low-index planes of CoP with and without N doping. b) Geometric configuration of H adsorption on the CoP (101) surface. c) Bader charge analysis and their differences to purely ionic models (ΔQ). d) Calculated DOS of Co atoms on the CoP (101) surface prior to and after N doping.

weakening adsorption.^[18,43] This trend is verified by choosing several other low-index crystal planes to study the changes in the surface hydrogen adsorption energy before and after the N doping (Figure 5a and Table S4, Supporting Information). We further examined the HER activities of the N-CoP samples with varied N doping positions and contents (Notes S6 and S7, Supporting Information) to study the influences of N dopants on catalytic activities via annealing experiments and theoretic DFT calculations (Notes S6–S8, Supporting Information). We found that there is an optimal value at 7.7% doping (anion basis) for the highest activity enhancement because of the H adsorption energy close to thermo-neutral states. Thus, the experimental and theoretic studies corroborate that N doping modulates the adsorption of H on the CoP surface to be more thermo-neutral and improve the catalytic performances for the HER.^[19,44]

The high electrocatalytic performances of CC@N-CoP encourage us to investigate the hydrogen production with even lower energy consumption. A coupled system consisting of an electrolyzer and an oxidation reactor is employed to produce hydrogen via HER and concurrently recover the useful sulfur resources. In the electrolyzer, H_2 gas evolves in the cathode compartment (Figure 6a), which is separated from the anodic compartment by a proton-exchange membrane as shown in Figure 6b. In the anodic compartment, Fe^{2+} is oxidized to Fe^{3+} . The redox couples of Fe^{3+}/Fe^{2+} are introduced to another absorption reactor in which Fe^{3+} oxidizes H_2S and

produces sulfur and protons (Figure 6c). The regenerated Fe^{3+}/Fe^{2+} couples and H^+ are recycled to the anodic compartment. Protons further diffuse through the Nafion membrane and evolve as H_2 in the cathode. We compared three electrolyzers: I) CC@N-CoP//CC in 0.5 M H_2SO_4 , II) CC@N-CoP//Pt in 0.5 M H_2SO_4 , and III) CC@N-CoP//CC in 0.5 M H_2SO_4 with 0.96 M $FeSO_4/0.74$ M $Fe_3(SO_4)_2$ (the electrodes on the left and right sides of “//” are the cathode and anode electrodes, respectively). Figure 6d shows that the first electrolyzer using CC@N-CoP//CC requires the voltage of as high as 1.91 V to drive the current of 10 mA cm^{-2} because CC has the low catalytic activity for the OER. In the second electrolyzer using CC@N-CoP//Pt, Pt is able to reduce the voltage to 1.76 V at 10 mA cm^{-2} . In the electrolyzer of the coupled system, OER is replaced with the oxidation reaction of Fe^{2+} . Overpotentials of electrolysis are significantly reduced. Only 0.89 V is able to drive the current density of 10 mA cm^{-2} . The energy consumption of the third electrolyzer decreases by 53% as compared to the first electrolyzer. The oxidized Fe^{3+} in the anodic compartment is introduced to react with H_2S in the absorption reactor (Figure 6c). The sulfur precipitate shows the crystallized XRD pattern which is in good agreement with α -S (JCPDS card 08-0247, Figure S20, Supporting Information).

A chronopotentiometric method is used to evaluate the long-term stability of the HER in the coupled system. During a 20 h test, the applied potentials increase nearly 20 mV (Figure 6e),

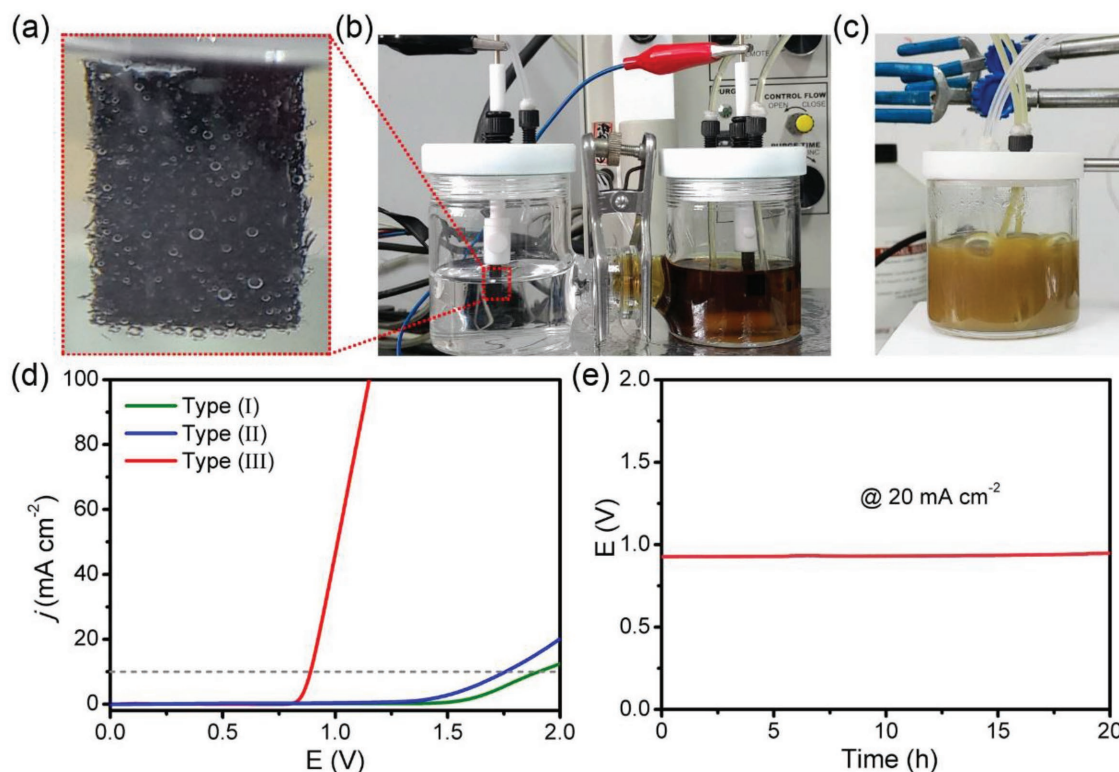


Figure 6. Coupled HER and sulfur productions: Optical photos of the coupled system: a) H₂ evolution, (b) electrolysis, and (c) H₂S absorption. d) LSV curves of three H₂ evolution electrolyzers: I) CC@N-CoP//CC in 0.5 M H₂SO₄, II) CC@N-CoP//Pt in 0.5 M H₂SO₄, and III) CC@N-CoP//CC in 0.5 M H₂SO₄ with 0.96 M FeSO₄/0.74 M Fe₃(SO₄)₂. e) Chronopotentiometric curve of the electrolyzer (III) using CC@N-CoP//CC and coupled H₂S absorption reactor working at 20 mA cm⁻².

indicating the good stability. The Faradaic efficiency of the HER is estimated by comparing the amount of evolved H₂ with the theoretical value (see Note S9, Supporting Information). The generated H₂ matches the theoretical value well. Figure S21 in the Supporting Information shows that the average Faradaic efficiency is ≈95.7% at varied current densities. The sulfur production efficiency is ≈95.1% (Figure S22, Supporting Information).

In conclusion, we developed a high-performance HER electrocatalyst by introducing nitrogen into orthorhombic CoP. Because of the strong electronegativity of nitrogen, the N dopants attract extra electrons from Co as compared to P and modulate the electron structure of CoP. The lowered d-band leads to the weakened adsorption of H on the surface of CoP and makes the free energy of adsorbed H (ΔG_{H^*}) closer to thermos-neutral states to enhance the HER activity. The overpotential for driving a current density of -10 mA cm⁻² is reduced to -42 mV, which is close to that of the benchmarking Pt catalyst for the HER. We further applied the newly developed HER catalyst for hydrogen and sulfur production in a coupled system. Because of the high catalyst activity of N-CoP and redox mediator, the energy consumption for hydrogen production via the HER is significantly reduced and useful sulfur sources are also recovered.

Supporting Information

Supporting Information is available from the Wiley Online Library or from the author.

Acknowledgements

The authors acknowledge the financial support of the National Science Foundation of China (21776121), Jiangsu Outstanding Youth Funds (BK20160012), “Jiangsu Shuanchuang” Program, Thousand Youth Talents Plan, National Materials Genome Project (2016YFB0700600), and Nantong Fundamental Research Funds (GY12016040). The numerical calculations in this paper have been done on the computing facilities in the High-Performance Computing Center (HPCC) of Nanjing University.

Conflict of Interest

The authors declare no conflict of interest.

Keywords

cobalt phosphide, electrocatalyst, hydrogen evolution reaction, nitrogen doping, sulfur recovery

Received: January 7, 2018

Revised: March 8, 2018

Published online:

[1] Z. W. Seh, J. Kibsgaard, C. F. Dickens, I. Chorkendorff, J. K. Nørskov, T. F. Jaramillo, *Science* **2017**, *355*, 6321.

[2] A. Ursua, L. M. Gandia, P. Sanchis, *Proc. IEEE* **2012**, *100*, 410.

- [3] I. Roger, M. A. Shipman, M. D. Symes, *Nat. Rev. Chem.* **2017**, *1*, 0003.
- [4] X. Zou, Y. Zhang, *Chem. Soc. Rev.* **2015**, *44*, 5148.
- [5] J. Wang, F. Xu, H. Jin, Y. Chen, Y. Wang, *Adv. Mater.* **2017**, *29*, 1605838.
- [6] Y. Jiao, Y. Zheng, M. Jaroniec, S. Z. Qiao, *Chem. Soc. Rev.* **2015**, *44*, 2060.
- [7] C. Yang, M. Y. Gao, Q. B. Zhang, J. R. Zeng, X. T. Li, A. P. Abbott, *Nano Energy* **2017**, *36*, 85.
- [8] C. G. Morales-Guio, L.-A. Stern, X. Hu, *Chem. Soc. Rev.* **2014**, *43*, 6555.
- [9] Y.-Y. Ma, C.-X. Wu, X.-J. Feng, H.-Q. Tan, L.-K. Yan, Y. Liu, Z.-H. Kang, E.-B. Wang, Y.-G. Li, *Energy Environ. Sci.* **2017**, *10*, 788.
- [10] a) J. Tian, Q. Liu, A. M. Asiri, X. Sun, *J. Am. Chem. Soc.* **2014**, *136*, 7587; b) C. Zhang, Y. Huang, Y. Yu, J. Zhang, S. Zhuo, B. Zhang, *Chem. Sci.* **2017**, *8*, 2769; c) H. Tabassum, W. Guo, W. Meng, A. Mahmood, R. Zhao, Q. Wang, R. Zou, *Adv. Energy Mater.* **2017**, *7*, 1601671; d) H. Yang, Y. Zhang, F. Hu, Q. Wang, *Nano Lett.* **2015**, *15*, 7616; e) C. Wu, Y. Yang, D. Dong, Y. Zhang, J. Li, *Small* **2017**, *13*, 1602873; f) H. Wang, S. Min, Q. Wang, D. Li, G. Casillas, C. Ma, Y. Li, Z. Liu, L.-J. Li, J. Yuan, M. Antonietti, T. Wu, *ACS Nano* **2017**, *11*, 4358.
- [11] a) C. Tang, R. Zhang, W. Lu, L. He, X. Jiang, A. M. Asiri, X. Sun, *Adv. Mater.* **2017**, *29*, 1602441; b) L. Yan, L. Cao, P. Dai, X. Gu, D. Liu, L. Li, Y. Wang, X. Zhao, *Adv. Funct. Mater.* **2017**, *27*, 1703455.
- [12] Q. Zhou, J. Pu, X. Sun, C. Zhu, J. Li, J. Wang, S. Chang, H. Zhang, *J. Mater. Chem. A* **2017**, *5*, 14873.
- [13] D. Y. Chung, S. W. Jun, G. Yoon, H. Kim, J. M. Yoo, K.-S. Lee, T. Kim, H. Shin, A. K. Sinha, S. G. Kwon, K. Kang, T. Hyeon, Y.-E. Sung, *J. Am. Chem. Soc.* **2017**, *139*, 6669.
- [14] S. Anantharaj, S. R. Ede, K. Sakthikumar, K. Karthick, S. Mishra, S. Kundu, *ACS Catal.* **2016**, *6*, 8069.
- [15] a) J. Wang, W. Cui, Q. Liu, Z. Xing, A. M. Asiri, X. Sun, *Adv. Mater.* **2016**, *28*, 215; b) T. Liu, X. Ma, D. Liu, S. Hao, G. Du, Y. Ma, A. M. Asiri, X. Sun, L. Chen, *ACS Catal.* **2017**, *7*, 98; c) R. Zhang, X. Wang, S. Yu, T. Wen, X. Zhu, F. Yang, X. Sun, X. Wang, W. Hu, *Adv. Mater.* **2017**, *29*, 1605502.
- [16] C. Tang, L. Gan, R. Zhang, W. Lu, X. Jiang, A. M. Asiri, X. Sun, J. Wang, L. Chen, *Nano Lett.* **2016**, *16*, 6617.
- [17] J. Kibsgaard, C. Tsai, K. Chan, J. D. Benck, J. K. Nørskov, F. Abild-Pedersen, T. F. Jaramillo, *Energy Environ. Sci.* **2015**, *8*, 3022.
- [18] T. Liu, D. Liu, F. Qu, D. Wang, L. Zhang, R. Ge, S. Hao, Y. Ma, G. Du, A. M. Asiri, L. Chen, X. Sun, *Adv. Energy Mater.* **2017**, *7*, 1700020.
- [19] P. Chen, T. Zhou, M. Zhang, Y. Tong, C. Zhong, N. Zhang, L. Zhang, C. Wu, Y. Xie, *Adv. Mater.* **2017**, *29*, 1701584.
- [20] P. Chen, T. Zhou, M. Chen, Y. Tong, N. Zhang, X. Peng, W. Chu, X. Wu, C. Wu, Y. Xie, *ACS Catal.* **2017**, *7*, 7405.
- [21] a) M. Caban-Acevedo, M. L. Stone, J. R. Schmidt, J. G. Thomas, Q. Ding, H.-C. Chang, M.-L. Tsai, J.-H. He, S. Jin, *Nat. Mater.* **2015**, *14*, 1245; b) B. Xia, L. An, D. Gao, S. Shi, P. Xi, D. Xue, *CrystEngComm* **2015**, *17*, 6420; c) J. Zhang, T. Wang, D. Pohl, B. Rellinghaus, R. Dong, S. Liu, X. Zhuang, X. Feng, *Angew. Chem.* **2016**, *128*, 6814; d) J. Wang, J. Liu, B. Zhang, X. Ji, K. Xu, C. Chen, L. Miao, J. Jiang, *Phys. Chem. Chem. Phys.* **2017**, *19*, 10125; e) W. Kohn, L. J. Sham, *Phys. Rev.* **1965**, *140*, A1133.
- [22] H. Li, C. Tsai, A. L. Koh, L. Cai, A. W. Contryman, A. H. Fragapane, J. Zhao, H. S. Han, H. C. Manoharan, F. Abild-Pedersen, J. K. Nørskov, X. Zheng, *Nat. Mater.* **2016**, *15*, 48.
- [23] B. You, X. Liu, N. Jiang, Y. Sun, *J. Am. Chem. Soc.* **2016**, *138*, 13639.
- [24] N. Jiang, B. You, R. Boonstra, I. M. Terrero Rodriguez, Y. Sun, *ACS Energy Lett.* **2016**, *1*, 386.
- [25] J. Wang, R. Kong, A. M. Asiri, X. Sun, *ChemElectroChem* **2017**, *4*, 481.
- [26] a) M. W. Kanan, D. G. Nocera, *Science* **2008**, *321*, 1072; b) C. Spöri, J. T. H. Kwan, A. Bonakdarpour, D. P. Wilkinson, P. Strasser, *Angew. Chem., Int. Ed.* **2017**, *56*, 5994.
- [27] a) C. Tang, R. Zhang, W. Lu, Z. Wang, D. Liu, S. Hao, G. Du, A. M. Asiri, X. Sun, *Angew. Chem.* **2017**, *129*, 860; b) D. Liu, T. Liu, L. Zhang, F. Qu, G. Du, A. M. Asiri, X. Sun, *J. Mater. Chem. A* **2017**, *5*, 3208.
- [28] a) J. Aali, O. Rahmani, *J. Pet. Sci. Eng.* **2012**, *86*, 217; b) G. Zhu, S. Zhang, Y. Liang, Q. Li, *Chin. Sci. Bull.* **2007**, *52*, 1394.
- [29] J. Shi, M. Zhang, D. Li, J. Liu, *Environ. Geochem. Health* **2018**, *40*, 915.
- [30] X. Zong, J. Han, B. Seger, H. Chen, G. Lu, C. Li, L. Wang, *Angew. Chem., Int. Ed.* **2014**, *53*, 4399.
- [31] F. Meng, H. Zhong, D. Bao, J. Yan, X. Zhang, *J. Am. Chem. Soc.* **2016**, *138*, 10226.
- [32] A. P. Grosvenor, S. D. Wik, R. G. Cavell, A. Mar, *Inorg. Chem.* **2005**, *44*, 8988.
- [33] a) A. W. Burns, K. A. Layman, D. H. Bale, M. E. Bussell, *Appl. Catal., A* **2008**, *343*, 68; b) M. Liu, J. Li, *ACS Appl. Mater. Interfaces* **2016**, *8*, 2158.
- [34] Y. Shi, B. Zhang, *Chem. Soc. Rev.* **2016**, *45*, 1529.
- [35] R. Ma, Y. Zhou, Y. Chen, P. Li, Q. Liu, J. Wang, *Angew. Chem., Int. Ed.* **2015**, *54*, 14723.
- [36] Y. Yin, J. Han, Y. Zhang, X. Zhang, P. Xu, Q. Yuan, L. Samad, X. Wang, Y. Wang, Z. Zhang, P. Zhang, X. Cao, B. Song, S. Jin, *J. Am. Chem. Soc.* **2016**, *138*, 7965.
- [37] a) M. S. Faber, R. Dziejczak, M. A. Lukowski, N. S. Kaiser, Q. Ding, S. Jin, *J. Am. Chem. Soc.* **2014**, *136*, 10053; b) D.-Y. Wang, M. Gong, H.-L. Chou, C.-J. Pan, H.-A. Chen, Y. Wu, M.-C. Lin, M. Guan, J. Yang, C.-W. Chen, Y.-L. Wang, B.-J. Hwang, C.-C. Chen, H. Dai, *J. Am. Chem. Soc.* **2015**, *137*, 1587; c) F. Wang, Y. Li, T. A. Shifa, K. Liu, F. Wang, Z. Wang, P. Xu, Q. Wang, J. He, *Angew. Chem.* **2016**, *128*, 7033.
- [38] a) J. D. Benck, Z. Chen, L. Y. Kuritzky, A. J. Forman, T. F. Jaramillo, *ACS Catal.* **2012**, *2*, 1916; b) J. Kibsgaard, Z. Chen, B. N. Reinecke, T. F. Jaramillo, *Nat. Mater.* **2012**, *11*, 963; c) J. Kibsgaard, T. F. Jaramillo, *Angew. Chem., Int. Ed.* **2014**, *53*, 14433.
- [39] J. Greeley, T. F. Jaramillo, J. Bonde, I. Chorkendorff, J. K. Nørskov, *Nat. Mater.* **2006**, *5*, 909.
- [40] R. Wu, J. Zhang, Y. Shi, D. Liu, B. Zhang, *J. Am. Chem. Soc.* **2015**, *137*, 6983.
- [41] J. K. Nørskov, T. Bligaard, J. Rossmeisl, C. H. Christensen, *Nat. Chem.* **2009**, *1*, 37.
- [42] a) Y. Hou, M. Qiu, T. Zhang, X. Zhuang, C.-S. Kim, C. Yuan, X. Feng, *Adv. Mater.* **2017**, *29*, 1701589; b) Z.-L. Wang, X.-F. Hao, Z. Jiang, X.-P. Sun, D. Xu, J. Wang, H.-X. Zhong, F.-L. Meng, X.-B. Zhang, *J. Am. Chem. Soc.* **2015**, *137*, 15070; c) C. Tsai, K. Chan, J. K. Nørskov, F. Abild-Pedersen, *Surf. Sci.* **2015**, *640*, 133.
- [43] a) B. Hammer, O. H. Nielsen, J. K. Nørskov, *Catal. Lett.* **1997**, *46*, 31; b) L. Yang, Z. Guo, J. Huang, Y. Xi, R. Gao, G. Su, W. Wang, L. Cao, B. Dong, *Adv. Mater.* **2017**, *29*, 1704574; c) B. Hammer, J. K. Nørskov, *Nature* **1995**, *376*, 238.
- [44] a) P. Chen, T. Zhou, M. Chen, Y. Tong, N. Zhang, X. Peng, W. Chu, X. Wu, C. Wu, X. Xie, *ACS Catal.* **2017**, *7*, 7405; b) S. Deng, Y. Zhong, Y. Zeng, Y. Wang, Z. Yao, F. Yang, S. Lin, X. Wang, X. Lu, X. Xia, J. Tu, *Adv. Mater.* **2017**, *29*, 1700748; c) N. Han, K. R. Yang, Z. Lu, Y. Li, W. Xu, T. Gao, Z. Cai, Y. Zhang, V. S. Batista, W. Liu, X. Sun, *Nat. Commun.* **2018**, *9*, 924; d) W. Xiao, P. Liu, J. Zhang, W. Song, Y. P. Feng, D. Gao, J. Ding, *Adv. Energy Mater.* **2017**, *7*, 1602086.